



Queensland University of Technology
Brisbane Australia

This is the author's version of a work that was submitted/accepted for publication in the following source:

[De Pellegrin, Dennis & Hargreaves, Douglas](#) (2012) An isoviscous, isothermal model investigating the influence of hydrostatic recesses on a spring-supported tilting pad thrust bearing. *Tribology International*, 51, pp. 25-35.

This file was downloaded from: <http://eprints.qut.edu.au/61821/>

© Copyright 2012 Elsevier

This is the author's version of a work that was accepted for publication in *Tribology International*. Changes resulting from the publishing process, such as peer review, editing, corrections, structural formatting, and other quality control mechanisms may not be reflected in this document. Changes may have been made to this work since it was submitted for publication. A definitive version was subsequently published in *Tribology International*, [VOL: 51, (2013)] DOI: 10.1016/j.triboint.2012.02.008

Notice: *Changes introduced as a result of publishing processes such as copy-editing and formatting may not be reflected in this document. For a definitive version of this work, please refer to the published source:*

<http://dx.doi.org/10.1016/j.triboint.2012.02.008>

The influence of hydrostatic recesses on spring-supported tilting pad thrust bearings

Dennis V. De Pellegrin^{*}, Doug J. Hargreaves

Queensland University of Technology, School of Engineering Systems
2 George St, Brisbane, Queensland, Australia

Abstract

Tilting-pad hydrodynamic thrust bearings are used in hydroelectric power stations around the world, reliably supporting turbines weighing hundreds of tonnes, over decades of service. Newer designs incorporate hydrostatic recesses machined into the sector-shaped pads to enhance oil film thickness at low rotational speeds. External pressurisation practically eliminates wear and enhances service life and reliability. It follows that older generating plants, lacking such assistance, stand to benefit from being retrofitted with hydrostatic lubrication systems. The design process is not trivial however. The need to increase the groove size to permit spontaneous lifting of the turbine under hydrostatic pressure, conflicts with the need to preserve performance of the original plane pad design. A haphazardly designed recess can induce a significant rise in bearing temperature concomitant with reduced mechanical efficiency and risk of thermal damage. In this work, a numerical study of a sector-shaped pad is undertaken to demonstrate how recess size and shape can affect the performance of a typical bearing.

Keywords: Tilting pad bearings; hydrostatic lubrication; hydroelectric power generation

^{*} Corresponding author. Tel: +61 7 3138 1615, Fax: +61 7 3138 1516, E-mail: d.depellegrin@qut.edu.au

Nomenclature

A_r	Overall recess area including tapered lands (Fig. 4)	[m ²]
B	Average sector arc length	[m]
F_x, F_y	Frictional force in x - and y -directions	[N]
$h(x,y)$	Oil film thickness at position (x,y)	[m]
h_i, h_o	Oil film thickness at pad inlet and outlet	[m]
$h_{i,j}$	Oil film thickness at node (i,j)	[m]
h_{nom}	Height between runner and pad plane measured at the spring centroid	[m]
h_{min}	Height between runner and outer trailing edge of pad	[m]
H	Inlet to outlet oil film thickness ratio (h_i/h_o)	
K	Convergence ratio (h_i/h_o-1)	
K_α	Convergence ratio with h_i and h_o measured along x -axis	
K_β	Convergence ratio with h_i and h_o measured along y -axis	
l_c	Capillary length (Eq. 4)	[m]
L_{ki}, L_{ko}	Inner and outer max taper depth (Fig. 4)	[m]
L_L, L_T	Pad leading- and trailing-edge truncation lengths (Fig. 2)	[m]
L_{sli}, L_{slo}	Length of inner and outer taper (Fig. 4)	[m]
N	Rotational speed	[rev·min ⁻¹]
N_s	Number of springs supporting one pad	
N_p	Number of pads that make up the thrust bearing	
M	Number of nodes	
$o-xy$	Groove-based rectangular coordinate system (Fig. 4)	
$O-XY$	Bearing-based rectangular coordinate system (Fig. 2)	
$p(x,y)$	Pressure at position (x, y)	[Pa]
$p_{i,j}$	Pressure at node (i,j)	[Pa]

p_r	Recess pressure (post capillary)	[Pa]
p_s	Oil supply pressure (pre capillary)	[Pa]
q	Oil flow rate per unit length	$[\text{m}^2 \cdot \text{s}^{-1}]$
Q	Oil flow across a boundary	$[\text{m}^3 \text{ s}^{-1}]$
Q_c	Oil flow rate through capillary (Eq. 4)	$[\text{m}^3 \text{ s}^{-1}]$
Q_e	Oil flow rate past leading pad edge (Eq. 8)	$[\text{m}^3 \text{ s}^{-1}]$
R^2	Correlation coefficient	
R_e	Recess outer radius (Fig. 4)	[m]
R_i, R_o	Inner and outer radii of sector-shaped pad (Fig. 2)	[m]
R_g	Radius of annular-segment groove (Fig. 4)	[m]
U	Bearing sliding velocity in x -direction $U=U_1+U_2$ (Eq. 1)	$[\text{m} \cdot \text{s}^{-1}]$
U_1, U_2	Pad and runner surface velocities in x -direction (Fig. 3)	$[\text{m} \cdot \text{s}^{-1}]$
V	Bearing sliding velocity in y -direction $V=V_1+V_2$ (Eq. 1)	$[\text{m} \cdot \text{s}^{-1}]$
V_1, V_2	Pad and runner surface velocities in y -direction (Fig. 3)	$[\text{m} \cdot \text{s}^{-1}]$
W, W_p	Total bearing and pad thrust loads	[N]
Γ_p	Frictional torque due to viscous drag contributed by one pad (Eq. 6)	$[\text{N} \cdot \text{m}]$
η	Dynamic viscosity (Eq. 1)	$[\text{Pa} \cdot \text{s}]$
θ	Isothermal temperature	[K]
$\Delta\theta$	Predicted average oil film temperature rise (Eq. 8)	[K]
κ	Spring stiffness	$[\text{N m}^{-1}]$
κ_z	Pad stiffness in z -direction	$[\text{N m}^{-1}]$
κ_α	Pad angular stiffness about y -axis (Eq. 15)	$[\text{N} \cdot \text{m} \cdot \text{rad}^{-1}]$
κ_β	Pad angular stiffness about x -axis (Eq. 15)	$[\text{N} \cdot \text{m} \cdot \text{rad}^{-1}]$
$o-\zeta\varepsilon$	Rectangular coordinate system aligned with leading pad edge (Eq. 10)	
ρ	Oil density (Eq. 8)	$[\text{kg} \cdot \text{m}^{-3}]$

Π_p	Power loss per pad due to viscous shear (Eq. 7)	[W]
σ	Oil specific heat (Eq. 8)	[J·kg ⁻¹ ·K ⁻¹]
ψ	Half-sweep of pad sector (Fig. 2)	[rad]
ω	Bearing (runner) angular velocity (Eq. 7)	[rad·s ⁻¹]

1. Introduction

Tilting pad thrust bearings commonly used in hydroelectric turbine installations are capable of supporting great loads with low friction and negligible wear, vibration and noise. A common arrangement is shown schematically in Fig. 1. The thrust bearing consists of a number of sector-shaped pads supported by springs that permit the pads to tilt relative to the runner. The convergent profile that is generated creates a pressurised oil film sufficiently thick so as to completely separate the sliding surfaces. The geometry of the bearing, combined with its structural attributes, loading, sliding velocity and oil viscosity, all govern the exact thickness of the oil film.

The main concern of the bearing designer is to minimise friction as it is not just a source of mechanical inefficiency but also a source of heat that, if not dissipated effectively, has the potential to degrade both the lubricating oil and the bearing surfaces. Although a properly designed hydrodynamic thrust bearing can operate with low coefficients of friction in the range 0.001–0.005, the enormous load typically supported means that heat generated in the oil film can be several kilo-Watts, which can manifest itself as an alarming rise in the oil film temperature.

Another practical problem for the bearing designer is how to deal with start-up and shut-down conditions when the bearing velocities approach zero. Solid-to-solid contact and the corresponding spike in friction coefficient must be accommodated without catastrophic damage to the bearing. In modern installations hydrostatic

lubrication solves this problem. External pressurisation by a pump forces oil into a recess machined into the pad surface. The flow of pressurised oil across the bearing lands creates sufficient thrust to separate the bearing surfaces completely. Hydrostatic pressurisation ceases once rotational velocity is sufficient to generate self-sustaining hydrodynamic pressures.

Modern installations are designed from the outset to accommodate hydrostatic recesses (e.g. [1, 2]) consisting primarily of a circular groove cut into each pad's planar surface and fed by a pressurised oil conduit. This type of recess is commonly used because it minimises pad distortion and recess volume. There is an incentive to minimise the dimension of the groove so as to limit performance deviations from that of the plane pad under hydrodynamic conditions.

In older installations, the absence of hydrostatic assistance makes turbine start-up and shut-down events of critical importance to the long-term integrity of the thrust bearing. Despite the obvious concerns, such installations have performed satisfactorily for decades thanks to precise operating procedure and thoughtful design. For example, by jacking the turbine off the pads momentarily after prolonged stationary periods and limiting bearing pressure at start-up to 1.5 MPa for whitemetal-lined pads [3]. Increasing demand for operational flexibility, requiring increased start-up and shut-down frequency, raises the potential for rapid bearing deterioration. This reliability risk could easily be eliminated by retrofitting the bearings with hydrostatic capability.

Careful consideration of the operating characteristics of a bearing must be made prior to adding any sort of hydrostatic recess. The presence of the recess inevitably affects the oil film thickness, and consequently the frictional power dissipation. Most interesting is the fact that the presence of a pocket may actually improve hydrodynamic bearing performance [4], but in other circumstances it may actually deteriorate bearing

performance by tilting the pad the wrong way [2, 5]. The potentially disastrous consequences of the latter would discourage many an engineer from considering the introduction of any sort of groove into a plane pad's surface.

Faced with this same prospect, the author devised a hydrodynamic simulation of a typical spring-supported pad to investigate the impact of adding a hydrostatic recess. The results were particularly interesting insofar as the groove could actually promote oil film thickness and reduce power loss at low angular velocity and lubricant viscosity relative to the plane pad baseline. Above a certain threshold of angular velocity and viscosity the converse was observed; but fortunately the negative effects are self-limiting insofar as rising temperature causes viscosity to decrease. The work presented herein investigates this phenomenon using a rigid pad, isoviscous model solved using the finite difference technique, and considers the potential to reduce frictional losses through the use of hydrostatic recesses.

2. Theory and Development

Effective hydrodynamic lubrication requires a viscous lubricant, a velocity difference and a convergent flow path between two surfaces. Theory for plane pad bearings indicates that a critical parameter that determines performance is the convergence ratio, $K = (h_i - h_o)/h_o$ [e.g. 5, 6], where h_i and h_o are the inlet and outlet oil film thicknesses respectively. For an 'infinite' planar pad bearing, the theoretical optimum value of K for maximum load carrying capacity is close to 1.2, whereas for minimising friction it is near 1.5. These values hold reasonably well for finite bearings provided the length-to-width-ratio (L/B) is no less than unity. For sector-shaped pads, maximum load carrying capacity occurs for values of K (h_i and h_o are defined at the mean radius of the sector) between 2 and 4 [7].

Complicating factors which cause deviations from theoretical formulations include thermal and mechanical distortion of the pad, and changing oil viscosity due to frictional heating. While these factors should be considered for accurate prediction of performance, they add significantly to the computational workload. An isoviscous rigid-pad model was used in this work on the basis that thermo-elastic pad deflection and thermally induced viscosity reductions have a stabilising effect that makes the recessed pad's performance converge back towards that of the plane pad under purely hydrodynamic conditions.

The benefit of using tilting pad bearings relative to fixed-geometry pads is that near-optimum values of K can be maintained regardless of load, speed and lubricant viscosity, as demonstrated theoretically in [6]. Pads may be pivoted along a line, a point, or suspended on an array of springs. The latter solution is used for large pads whereby the springs limit pad bending moments by counteracting the hydrodynamic forces with a more evenly distributed pressure on the underside of the pad [8].

2.1 Pressure modelling

In rotating equipment, axial thrust forces can be counteracted by using sector shaped pads, arranged as per Fig. 1. Sector-shaped pads may be considered homologous to a rectangular pad. The number of pads used typically ranges from three upwards. Unlike the rectangular pad, the velocity varies in both magnitude and direction across the face of the sector. Optimisation of a sector-shaped pad is also more complex than for a rectangular pad. Although it is possible to obtain reasonable estimates by approximating the sector-shaped pad to a rectangular pad with width equal to average arc-length B , and length equal to the radial extent ($R_o - R_i$), the errors can be significant. The use of graphical or tabular bearing performance data is often convenient (e.g. [7]), however it

may be difficult to find correspondence with the design being considered. The final alternative is to model the problem using numerical methods to solve the exact geometry as required.

Typically, a polar coordinate formulation of Reynolds' equation would suit the sector-shaped bearing (e.g. [7]), however, the pad studied in this instance is not strictly sector-shaped as it is generated by cutting the trailing edge of the pad with lines parallel to the radials, as shown in Fig. 2. Such a pad is here onwards called a *truncated sector*. As a consequence of this added complexity, the solution method is based on the finite difference method using a rectangular coordinate system, with fine enough divisions to accurately reflect both the angled and curved boundaries of the pad.

Reynolds' equation in rectangular coordinates is given by,

$$\frac{\partial}{\partial x} \left(h^3 \frac{\partial p}{\partial x} \right) + \frac{\partial}{\partial y} \left(h^3 \frac{\partial p}{\partial y} \right) = 6\eta \left(U \frac{\partial h}{\partial x} + V \frac{\partial h}{\partial y} \right) \quad (1)$$

where η is the isoviscous dynamic viscosity and $U = U_1 + U_2$ and $V = V_1 + V_2$ are the sum surface velocities in x - and y -directions respectively, as defined in Fig. 3 for a rectangular bearing (U_1 and V_1 both equal 0). For the thrust bearing in question, runner velocities U and V are functions of position (x,y) and angular velocity, ω . It may be shown that U is not a function of x and that V is not a function of y , which means that the terms U and V can be moved outside of their respective differential operators to give Eq (1). Due to the incongruous shape of the truncated sector relative to the polar coordinate system, no attempt was made to generalise the solution in dimensionless terms.

2.2 Solving the pressure field

The numerical solution was obtained by making finite difference substitutions for the first and second derivatives of pressure using first order Taylor expansion approximations. The resulting expression was then simplified in terms of the nodal pressures to the following finite difference expression,

$$p_{i,j} = \frac{\frac{p_{i+1,j} + p_{i-1,j}}{\delta x^2} + \frac{p_{i,j+1} + p_{i,j-1}}{\delta y^2} + \frac{3}{h} \left[\frac{\partial h}{\partial x} \left(\frac{p_{i+1,j} - p_{i-1,j}}{2\delta x} \right) + \frac{\partial h}{\partial y} \left(\frac{p_{i,j+1} - p_{i,j-1}}{2\delta y} \right) \right] - \frac{6\eta}{h^3} \left(U \frac{\partial h}{\partial x} + V \frac{\partial h}{\partial y} \right)}{\frac{2}{\delta x^2} + \frac{2}{\delta y^2}} \quad (2)$$

where δx and δy are length dimensions of the grid elements in x - and y -directions respectively. The pressure at each node (i,j) may be calculated iteratively using the pressures immediately surrounding to the north $(j+1)$, south $(j-1)$, east $(i+1)$ and west $(i-1)$, together with the local velocity, film thickness and gradients in x - and y -directions. This is effectively the Gauss-Seidl method as described for example in [8].

2.3 Consequences of adding the hydrostatic recess

A toroidal-segment groove with tapered relief on both sides is shown in Fig. 4. Justification for this shape and the size of the parametrically defined dimensions will be elaborated upon in a subsequent section.

Finite difference solution of Reynolds' equation using the Gauss-Seidl method works well for pads with planar faces where film gradients are small. The presence of any type of closed groove of depth significantly greater than the average film thickness can inhibit solution convergence. This occurs because hydrodynamic pressures cannot propagate from the boundary conditions across rapid changes in oil film thickness. The region inside the recess is completely surrounded by the groove and hence, the establishment of correct pressure within the recess requires equilibration of fluid flow to satisfy the condition of mass conservation.

This problem is resolved by adjusting the pressure at the oil supply hole until the net oil flow rate across any closed boundary is zero. Under hydrostatic conditions, the set boundary pressure at the oil supply hole overcomes this problem automatically, as the pressure can expand from within the groove to meet the propagation front originating from the pad extremity. Under pure hydrodynamic conditions, however, the pressure at the nodes within the groove appears to be pinned to the initialised pressure (typically zero Pascals). This phenomenon is evidently in contrast with reality and needs to be solved by providing an artificial internal boundary condition at the oil hole. Instead of the pressure being set by the capillary characteristics and oil flow rate, the pressure is varied up or down until the net oil flow across the bearing boundary equals zero. This ensures that conservation of mass is satisfied as the net oil flow rate across the pad boundary must equal zero when the hydrostatic supply is switched off.

The choice of recess shape and profile is based on a number of constraints imposed by the original bearing design. For example, specifications might require that the bearing: (a) levitate the rotor by hydrostatic pressure alone without external assistance, (b) be fully machined within the Babbitt lining, and (c) not degrade performance as compared to the originally designed plane pad.

The condition of self-levitation

When the bearing is stationary the levitating force is the product of oil pressure times the projection area over which it acts. When the bearing is pressed against the runner (with sufficient time having passed for the oil film to have squeezed out and neglecting manufacturing defects such as roughness or waviness) this area corresponds to the projection of the recess. It is easy to overlook the fact that outside the recess hydrostatic oil pressure is zero. Initial oil flow is hindered by the fact that the runner is very smooth

and the pad lining is very soft, sealing the pressurised oil from flowing across the pad face. Oil flow can only occur via capillary action through surface defects, or if the pad and runner are momentarily separated. To rely on surface roughness and manufacturing defects to provide the initial film would provide erratic results.

Alternatively, it would be sufficient to use external jacks to prime the film by momentarily lifting the rotor off the pads. However, it is often desirable to eliminate the complexity of fixed hydraulic jacks. Even an instantaneous torque of sufficient magnitude would be enough to enable hydrostatic lift-off, as the relative movement of the surfaces would create paths for the oil to flow into out of the recess.

In this work, the groove is made sufficiently large so that hydrostatic lift-off can occur spontaneously with modest oil pressure that is unlikely to cause spalling or plastic flow in the Babbitt lining. It is noted that the compressive yield strength of Babbitt metals, which at 20°C, ranges from 40–60 MPa, can reduce by up to 50% at 100°C [9]. In order to achieve this, the groove is extended with a tapered profile on both the inside and the outside (again the reader is referred to Fig. 4).

In this study, different combinations of groove and taper, possessing identical projected recess areas, are examined for their influence on bearing performance. As will be demonstrated in the results section, it is preferable to have a larger diameter groove but reduce or eliminate the outer taper. The inner taper on the other hand can have a beneficial effect as the torque that it induces tends to reduce friction for this specific example, i.e. the original plane pad convergence is well below optimal.

Groove size limitation

The allowable depth of the groove size is limited here by the thickness of the Babbitt metal lining (3 mm in this instance). Cutting past the Babbitt into the mild steel exposes

the interface to hydraulic pressures that could spall the lining during hydrostatic lift-off. This is a serious problem that prevails when hydrostatic pressure is not restricted. The rounded profile reduces stress concentrations when compared to a square cut.

Minimising impact on original bearing performance

The introduction of a hydrostatic recess can have significant impact on bearing performance under the full range of hydrodynamic operating conditions. In order for the degradation of performance to be minimised it is ideal to position the groove so that it follows an isobar of the plane hydrodynamic pad [4]. This has been achieved approximately by making the groove centroid coincide with the spring centroid. Moving the groove further towards the pressure peak presents the risk that the pad might not completely levitate under hydrostatic operation, or that a divergent rather than a convergent film profile results.

The presence of the groove changes the pressure distribution, which affects pad tilt relative to the original planar pad geometry. The danger is that the bearing will run hotter due to increased viscous shear, or in the extreme case that the pad will tilt forwards and the oil film collapse.

A numerical simulation to visualise the impact of groove geometry on pad tilt is therefore highly valuable, as it facilitates observation of the impact that the presence of the groove has on performance relative to the original plane pad design.

2.4 Setting the solution domain

A rectangular domain is defined that envelopes the entire pad geometry. Although costly in terms of memory storage, pressure calculations are only conducted on nodes that fall within the pad domain. The pressure is set to zero for those nodes that fall

outside of the pad boundary, thereby defining valid boundary conditions. The nodes falling within the region of the oil supply hole are set to a suitable pressure depending on whether hydrostatic supply is activated or deactivated. The nodal oil film height $h_{i,j}$ is calculated at the start of each simulation from the parametrically defined pad, recess geometry, and the initial height and orientation of the pad.

Repeated calculation of Eq. (2) over all nodes within the pad domain yields a pressure distribution that converges towards equilibrium. The pressure field is numerically integrated over the pad domain to obtain pad load and moments. If the load supported by the bearing is lower/higher than rotor weight and hydraulic force combined, then the pad position is reduced/raised while maintaining the pad convergence constant in both x - and y -directions. This last detail emulates reality and achieves much faster load convergence.

The decision to raise or lower the pad is based on a heuristic rule that considers as input the sign of the load error and both its first and second derivative. Maximum height compensation occurs when the error is positive, increasing and accelerating. Height is not changed, for example, if error is positive but both decreasing and decelerating. This simple rule results in effective, stable convergence when the step height change is suitably small ($\Delta h_{\text{nom}} \sim 10^{-8}$ m).

Once the load error is within the designated error margin, the pad moments are balanced by appropriately incrementing or decrementing convergence in both x and y directions and repeating the load convergence cycle until equilibrium is obtained to within a small margin of error.

2.5 Calculating the oil flow rate

Oil flow can be calculated theoretically by,

$$Q_x = \int q_x dy = \int_{y_1}^{y_2} \left[-\frac{h^3}{12\eta} \frac{\partial p}{\partial x} + \frac{Uh}{2} \right] dy \approx \sum_{j_1}^{j_2} \left[-\frac{h^3}{12\eta} \frac{\partial p}{\partial x} + \frac{Uh}{2} \right] \delta y \quad (3a)$$

$$Q_y = \int q_y dx = \int_{x_1}^{x_2} \left[-\frac{h^3}{12\eta} \frac{\partial p}{\partial y} + \frac{Vh}{2} \right] dx \approx \sum_{i_1}^{i_2} \left[-\frac{h^3}{12\eta} \frac{\partial p}{\partial y} + \frac{Vh}{2} \right] \delta x \quad (3b)$$

The pad oil flow Q is easily calculated by numerical integration across the four edges of a rectangular boundary aligned with the xy -coordinate system. In this instance, the rectangle was conveniently located in the region between the recess boundary and the pad boundary. Here the pressure gradients are not subject to extreme changes so the numerical error of the calculated oil flow is reduced to a small value.

In pure hydrodynamic lubrication, net oil flow across any closed boundary must equal zero, which provides a valuable check that the mathematics have been implemented correctly. Under hydrostatic conditions, there must be a balance between the oil flowing out of the rectangular boundary and that supplied through the oil hole. The pressure at the groove supply hole was therefore calculated according to pump delivery pressure, net oil flow, lubricant viscosity and capillary specifications.

2.6 Capillary flow

Modelling of the hydrostatic oil flow requires detailed understanding of the pump and oil supply system. Typically, hydraulic pumps are positive displacement devices whereby flow rate is closely related to drive speed. This oil flow is reduced with increasing outlet pressure due to vane-leakage and the torque-speed characteristics of the motor.

It is convenient to model the pump as a constant pressure supply. This can be achieved by means of a by-pass valve. The supply pressure will therefore remain

approximately constant provided that the pump oil flow capacity always exceeds the oil flow demanded by the device, in this case the hydrostatic bearing. When the bypass valve is not activated, bearing supply pressure p_s will be governed by the pump characteristics and back pressure.

The oil flow is restricted by a capillary for each pad which limits the oil flow rate. The pressure drop from supply side to pad recess side ($\Delta p_c = p_s - p_r$) may be described by,

$$\Delta p_c = \frac{128l_c}{\pi d_c^4} Q_c \eta \quad (4)$$

where d_c is the capillary diameter, l_c is the length and Q_c is the oil flow rate through the capillary that supplies the pad recess. This is the Hagen-Poiseuille equation and applies for $l/d > 100$ and laminar flow, i.e. Reynolds number < 2300 .

The oil flow rate Q_c must equal the oil flow across any boundary between the recess and pad edge, calculated using Eq. (4). Iterative solution and readjustment of the recess supply pressure finally results in solution convergence.

2.7 Frictional torque and power dissipation

The friction force contribution at each node, as seen by the runner, can be calculated by,

$$\delta F_x = \left[-\frac{h}{2} \frac{\partial p}{\partial x} - \frac{U\eta}{h} \right] \delta x \delta y \quad (5a)$$

$$\delta F_y = \left[-\frac{h}{2} \frac{\partial p}{\partial y} - \frac{V\eta}{h} \right] \delta x \delta y \quad (5b)$$

and the frictional torque contributed by one pad to the overall bearing torque may be calculated by,

$$\Gamma_p = \sum_{i=1}^M (\delta F_{y,i} \cdot X_i - \delta F_{x,i} \cdot Y_i) \quad (6)$$

where $(1..M)$ represents all the nodes in the domain. The power dissipated by friction is calculated by,

$$\Pi_p = \Gamma_p \cdot \omega \quad (7)$$

2.8 Estimating the oil film temperature rise under hydrodynamic conditions

A simple estimation of average oil temperature rise $\Delta\theta$, assuming adiabatic conditions, may be calculated by equating the frictional power dissipated in the pad and the convective heat flow rate into the fluid, as per [10],

$$\Pi_p = Q_e \rho \sigma \Delta\theta \quad (8a)$$

$$\Delta\theta = \frac{\Pi_p}{Q_e \rho \sigma} \quad (8b)$$

where ρ is the density of oil, σ is the specific heat of the oil, and Q_e is the oil flow rate entering the pad, which theoretically equals the oil flow rate past the leading edge of the pad.

The elemental oil flow rate into the pad is calculated from the flow equation,

$$\delta Q_e = \left[-\frac{h^3}{12\eta} \frac{\partial p}{\partial \zeta} + \frac{vh}{2} \right] \delta \varepsilon \quad (9)$$

where $o-\zeta\varepsilon$ is the local coordinate system rotated clockwise by ψ (negative value)

relative to $o-xy$, so as to align the ζ -axis perpendicular to the leading edge of the pad,

and,

$$v = U \cos \psi - V \sin \psi \quad (10)$$

$$\frac{\partial p}{\partial \zeta} = \frac{\partial p}{\partial x} \cos \psi - \frac{\partial p}{\partial y} \sin \psi \quad (11)$$

$$\delta \varepsilon = \frac{\delta y}{\sin \psi} \quad (12)$$

The total flow across the leading edge is therefore,

$$Q_e = \sum_{i=1}^M \delta Q_{e,i} \quad (13)$$

where $(1..M)$ is the sequence of nodes spanning the leading edge of the pad.

2.9 Calculating the spring centroid and pivot point

It is common practice to position the springs symmetrically about the bisecting Y -axis so that the spring centroid falls on the same line. The spring centroid (X_s, Y_s) is the point around which the pad pivots when an offset perpendicular force is applied. A force coinciding with the spring centroid, on the other hand, causes linear displacement but no rotation. This position is found by,

$$X_s = \frac{\sum_{i=1}^{N_s} X_i \kappa_i}{\sum_{i=1}^{N_s} \kappa_i} \quad (14a)$$

$$Y_s = \frac{\sum_{i=1}^{N_s} Y_i \kappa_i}{\sum_{i=1}^{N_s} \kappa_i} \quad (14b)$$

where (X_i, Y_i) is the spring's location and κ_i its stiffness.

The relative position between the spring and hydrodynamic pressure centroids, combined with the angular stiffness of the bearing determines how far the pad tilts. The angular stiffness in the y - and x -directions respectively can be calculated by,

$$\kappa_\alpha = \sum_{i=1}^{N_s} |Y_i - Y_s| \kappa_i \quad (15a)$$

$$\kappa_\beta = \sum_{i=1}^{N_s} |X_i - X_s| \kappa_i \quad (15b)$$

It is essential that a converging profile is generated for effective hydrodynamic lubrication. For this to occur the pressure centroid has to lead the spring centroid—a condition that is favoured by cutting the trailing edge of the pad so that it is shorter than the leading edge (refer to Fig. 2).

The placement of the recess is very important for hydrostatic lubrication. The hydrostatic pressure centroid should be close to the spring centroid so that the bearing and runner remain close to parallel. A bias towards a converging profile is always preferable as this assists the development of hydrodynamic lubrication once rotation begins. It is conceivable that complete separation of the surfaces might not occur if the hydrostatic pressure centroid exceeds some critical distance from the spring centroid. Such a condition would represent poor design.

3. Experimental Details

The scope of this work is limited to investigating the general behaviour of a bearing similar in design to that of an existing hydroelectric installation. Owing to the numerous degrees of freedom of this class of bearing, it is difficult to generalise the solutions obtained. Numerical simulation is therefore a highly beneficial tool for understanding the behaviour of new bearing designs.

3.1 The shape of the pad

The pads in the original bearing installation are planar, apart from a short taper on the leading edge and small radius on the trailing edge. A pad with approximately the same dimensions is shown in Fig. 2. The angular extent of the bearing ($\beta = 45^\circ$) coincides with the division of a full revolution by the number of pads—in this case eight. The pad length (radial extent) is 350 mm, while the width (circumferential extent) is 304 mm at the mean radius (445 mm).

3.2 The shape of the recess

The recess allows hydrostatically pressurised oil to prise apart the bearing and runner surfaces. The groove is significantly deeper than the expected film thickness, so the pressure within the groove may be considered constant under hydrostatic conditions. The tapered relief on either side of the groove provides a greater projected area for the hydrostatic film to act over in order to facilitate lift-off. The combined recess profile impacts bearing performance under hydrodynamic conditions. Table 1 gives the three cases studied in this work. All three recesses possess the same projected area, $A_r=13,000 \text{ mm}^2$, providing equal lift-off capability, but different hydrodynamic performance.

3.3 Bearing loading and pad stiffness

The bearing is loaded by the static weight of the rotor, i.e. 190 tonnes at start-up. The hydraulic force acting on the turbine adds another 85 tonnes of thrust. Fortunately, the hydrostatic thrust necessary at start-up is just the static rotor weight. Under fully loaded hydrodynamic conditions the thrust on each the pad is therefore $W_p = 340 \text{ kN}$.

Individual spring stiffness is 3 MN/m, which gives rise to 114 MN/m for the pad vertical stiffness which translates to 1.4 mm deflection when spring pre-load is taken into account. Angular stiffnesses are calculated around the y -axis, $\kappa_\alpha = 7.8 \text{ MNm/rad}$, and along x -axis, $\kappa_\beta = 9.4 \text{ MNm/rad}$.

3.4 Oil viscosity

The lubricating oil viscosity at 40°C is 0.057 Pa·s (65 cS) and at 100°C, 0.008 Pa·s (8.7 cS). The density of the oil is $870 \text{ kg}\cdot\text{m}^{-3}$. The oil is a mineral hydraulic oil with

viscosity-temperature characteristics interpolated from an ASTM D341 chart and tabulated in Table 2 for various operating temperatures.

3.5 Oil supply and capillary specifications

Under hydrostatic flow conditions the pump supply capability, bypass pressure and capillary characteristics determine oil film thickness. In the simulation the pump flow capacity was limited to 33.6 L/min and the bypass pressure set to 20 MPa. These figures are based on a sensible sizing of pump and drive motor. By limiting the oil flow rate, pumping power requirements are contained within reasonable levels. As a consequence hydrostatic oil film thickness starts dropping when the oil flow limit is breached. For example, the design nominal film thickness of 108 μm drops to 60 μm at 80°C for the current setup.

The flow from the pump feeds the bypass valve and filter followed by a distribution manifold. Each pad is fed from the distribution manifold via its own capillary. The capillary is 50 mm long and 1 mm in diameter, ($l/d = 50$) which is less than required for accuracy of the Hagen-Poiseuille equation however close enough given practical difficulty of drilling a longer capillary. At the higher temperatures ($>60^\circ\text{C}$) the flow in the capillary is estimated to be above the turbulent threshold. Both these factors increase the pressure drop compared to that predicted by the Hagen-Poiseuille model, somewhat degrading the oil film thickness calculated by the simulation. From a practical perspective, this is not a problem given the generous minimum film thickness allowed for.

3.6 Running the simulation

Various experiments were performed, however the variable of fundamental importance is the oil film thickness and how it varies with changing operating conditions such as recess design, speed and viscosity (temperature). Other variables recorded include: convergence, friction torque, average temperature rise and pressure distribution. Graphical output of the pad pressure distribution enables constant monitoring of solution convergence. Sample pressure distributions are shown for plane and recessed pads, under hydrodynamic and hydrostatic conditions, in Fig. 5. The size of the grid used for all calculations was 500×391 nodes.

4. Results and Discussion

The addition of a hydrostatic groove can have significant effects on the operation of a tilting pad hydrodynamic bearing. The simulation data is presented and discussed in this section.

4.1 Plane pad bearing performance

The performance of the plane pad bearing forms a baseline for comparison with hydrodynamic performance of recessed pads. Plane pad performance is shown in Fig. 6. The most important parameters include nominal film thickness h_{nom} (the height from the runner to bearing plane at the spring centroid) and the convergence ratio K_α (a measure of the ratio of inlet to outlet oil film thickness along the x -axis). Both these variables are governed by the product of viscosity and rotational speed ($\eta \cdot N$) shown on the abscissa. A 5% rise in viscosity, for example, has the same effect as a 5% rise in rotational velocity. A dimensionless abscissa variable including pressure in the denominator was

not used to avoid creating the impression that strict proportionality exists between the parameters.

It may be observed that proportionality of the nominal film thickness with the square root of $\eta \cdot N$ is well approximated. This relationship is predicted by the analytical solution of the infinite planar pad when convergence is assumed to be constant. The experimental convergence is not strictly constant (as predicted by infinite plane pad theory) but it is constrained within the band $K_\alpha = 0.4\text{--}0.8$ (Fig. 6).

It may be noted that the convergence ratio is well below the optimum value for maximising oil film thickness. It is anticipated that thermal effects cause pad convergence to increase, however not to the extent required for optimising load capacity, oil film thickness and friction coefficient. According to the isoviscous simulation, moving the spring centroid back about 20 mm causes the convergence ratio to increase from 0.65 to a value of 2, and the average oil film temperature rise ($\Delta\theta$) to drop from 32°C to 14°C for conditions otherwise identical to those illustrated in Fig. 7(a). The level of optimisation performed on such bearings, which often date back to the 1950's if not earlier, is questionable. There could be a strong economic argument for revising the design of older thrust bearings around the world.

4.2 Effect of groove shape on bearing performance

The addition of a hydrostatic recess impacts negatively upon bearing performance at high velocity and viscosity. Fortunately, the resulting temperature rise and associated reduction of viscosity tends to diminish this impact. Nonetheless, it is important to investigate the sensitivity of the bearing to these negative effects. The graphs in Fig. 7 illustrate that there is an increasing divergence from the plane pad baseline. At high values of $\eta \cdot N$, the rise in oil film thickness is comparatively diminished as is the

magnitude of the convergence ratio. This fall in convergence is associated with increasing frictional power loss and bearing temperature rise, as demonstrated by Fig. 8.

At low values of $\eta \cdot N$ the presence of the groove is actually beneficial to pad operation as it increases convergence, thus increasing nominal film thickness and reducing both friction and temperature rise.

Of the three recess designs, it is clear that design A has the most beneficial effect, insofar as it follows reasonably closely the plane pad baseline. Design C, on the other hand, exhibits unstable behaviour (collapse of the oil film) above $\eta \cdot N \approx 65 \text{ Pa} \cdot \text{s} \cdot \text{rev} \cdot \text{min}^{-1}$ owing to the excessive reduction of pad convergence. In reality, the associated oil film temperature rise and viscosity decrease would work towards stabilising pad convergence. Nonetheless the deviation from the plane pad performance for design C is a cause for concern.

The key feature of the different recess designs is the taper on the outer side of the groove. The projected areas of recesses A–C are otherwise identical. Type A has the groove with no outer taper, whereas type C has its groove centred at the radius of 45 mm and a taper extending out to the recess extremity. The reader is directed to Table 1 for details on groove dimensions.

Figure 7(a) shows that the recessed pad that offers performance most similar to the baseline is type A. The lack of outer taper in this design eliminates the leading and trailing pressure spikes otherwise seen with types B and C.

4.3 Groove type and the effect on pad temperature

The effect of recess geometry on bearing friction and temperature is clearly illustrated in Fig. 8 for the three different recess types. The external taper reduces the inclination of the pad at high $\eta \cdot N$ values. The more parallel the pad to the runner, the thinner the oil

film thickness, resulting in increased shearing and higher bearing temperatures. It is interesting to note that eliminating the outer taper provides the least impact on baseline performance, despite the fact that the groove diameter is the largest of the three cases.

A key observation is that it is best to avoid tapers outside the groove as these generate unfavourable pressure distributions that lead to a reduction of convergence ratio. The best course of action is to keep the grooves as small as possible subject to the demands of hydrostatic lubrication performance.

It may also be observed that dynamic viscosity and speed do not have the same proportional effect on power loss (note the irregularity of $\eta \times N$ versus Π_p in Fig. 8), as it does for pad convergence, film thickness and average film temperature rise.

4.4 General considerations

The mechanism by which the presence of the recess affects pad performance is illustrated in Fig. 9. It is possible to observe how the pressure distribution is changed when compared to the plane pad. The superposition of a torque on the pad leads to changed pad convergence, which impacts both film height and friction.

It is desirable to minimise the dimension of any tapered relief along the outside edge of the groove as this has negative impact on bearing performance. Any wear during service, or manufacturing defects that might introduce similar tapering, could further degrade bearing performance. For this reason, it is desirable to limit the size of the recess to a relatively small value, notwithstanding the impact this has on the capability of hydrostatic pressure to spontaneously lift the turbine off the bearing pads.

Despite the fact that rigid-pad, isoviscous simulations are limited in their representation of reality, they nonetheless provide a great deal of knowledge about bearing behaviour. Thermal crowning of the pad and the viscosity reduction at high

velocities reduce the negative impact of introducing a groove into the surface of a plane pad. This provides some comfort, but full confidence in simulation results can only be obtained with the inclusion of pad deformation and thermal effects and therefore this is a priority in future research.

5. Conclusions

From this work the following conclusions have been drawn:

- Adding hydrostatic assistance is beneficial for reducing friction and wear at start-up and very low rotational speeds.
- The presence of the recess can have both a positive and negative impact on performance when compared to a plane pad, with negative effects prevalent at high oil viscosity and bearing speed.
- The hydrostatic pocket should be made as small as possible subject to the minimum requirements for hydrostatic lubrication.
- Tapering externally to the groove should be avoided. It is preferable to increase the radius of the groove if a larger recess is required.
- Numerical simulation is indispensable for assessing the performance of complex, spring mounted tilting pad bearings with many degrees of freedom.
- The addition of thermo-elastic modelling to the simulation is seen as an important objective for future work.

References

- [1] Medley AL, Brown JB, Ferguson JH. Spring supported thrust bearings used in hydroelectric generators: Finite element analysis of pad deflection. In: Dalmaz G, Lubrecht AA, Dowson D, Priest M, editors. Tribology research: from model experiment to industrial problem, London: Elsevier; 2001, p.99-110.
- [2] Glavatskih S. Tilting pad thrust bearings. In: Dowson D. et al. (eds.), Tribological research and design for engineering systems, Boston: Elsevier; 2003. p.379–390.
- [3] Engineering Sciences Data Unit (ESDU), Calculation methods for steadily loaded, off-set pivot, tilting pad thrust bearings, Item 83004. London: ESDU International Ltd; 1983.
- [4] Wordsworth RA, Ettles CMM. The effect of jacking pockets in hydrodynamic thrust pads. *Wear* 1975; 31:167–171.
- [5] Cameron A. Basic Lubrication Theory, London: Ellis Horwood; 1981.
- [6] Stachowiak GW, Batchelor AW. Engineering tribology, Amsterdam: Elsevier; 1993.
- [7] Pinkus O, Sternlicht B. Theory of hydrodynamic lubrication, New York: McGraw Hill; 1961.
- [8] Khonsari MM, Booser ER. Applied Tribology: Bearing design and lubrication, Chichester: Wiley; 2008.
- [9] Klebanov BM, Barlam D, Nystrom FE. Machine elements: Life and design, CRC Press; 2007.
- [10] Williams JA. Engineering tribology, New York: Cambridge University Press; 2004.

Figure captions

- Fig. 1. Schematic illustration of a hydroelectric turbine installation, showing the thrust bearing and pad arrangement.
- Fig. 2. Plan view of the truncated sector pad, showing nominal spring positions and groove location.
- Fig. 3. Mathematical setup of bearing coordinate system.
- Fig. 4. Details of toroidal-segment oil supply groove with inner and outer tapered relief.
- Fig. 5. Rigid isoviscous pressure distributions for: (a) plane pad; (b) pad with type B recess; (c) pad with type B recess plus hydrostatic supply.
- Fig. 6. Nominal film thickness and convergence for the plane (un-recessed) pad as a baseline for comparison with recessed pads.
- Fig. 7. Nominal film thickness and convergence performance of recessed pads relative to a plane pad: (a) recess type A; (b) recess type B; (c) recess type C.
- Fig. 8. Average oil film temperature rise and frictional power loss of recessed pads relative to plane pad: (a) recess type A; (b) recess type B; (c) recess type C.
- Fig. 9. The variation of pressure profile across the pad (recess type C) in the x -direction (trailing edge on the left) under hydrodynamic condition showing the effect of increasing speed or dynamic viscosity under isoviscous conditions.

Table captions

- Table 1. Geometry specification of the three recess types (A, B and C) tested. Refer to Fig. 4 for symbol definitions.
- Table 2. Viscosity extrapolation of oil as per ASTM D341.

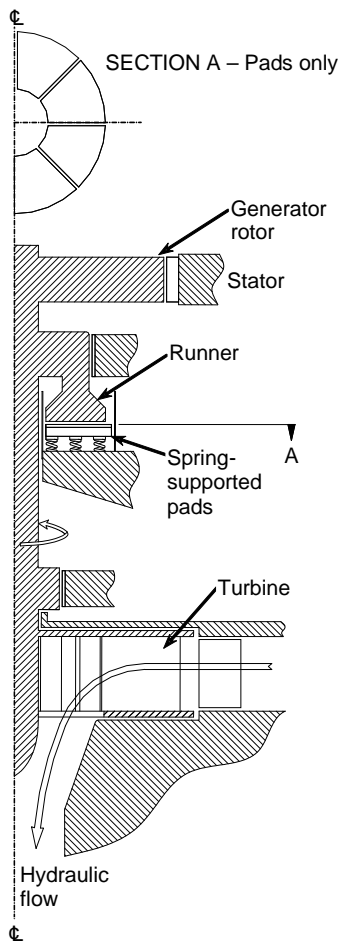


Fig. 1. Schematic illustration of a hydroelectric turbine installation, showing the thrust bearing and pad arrangement.

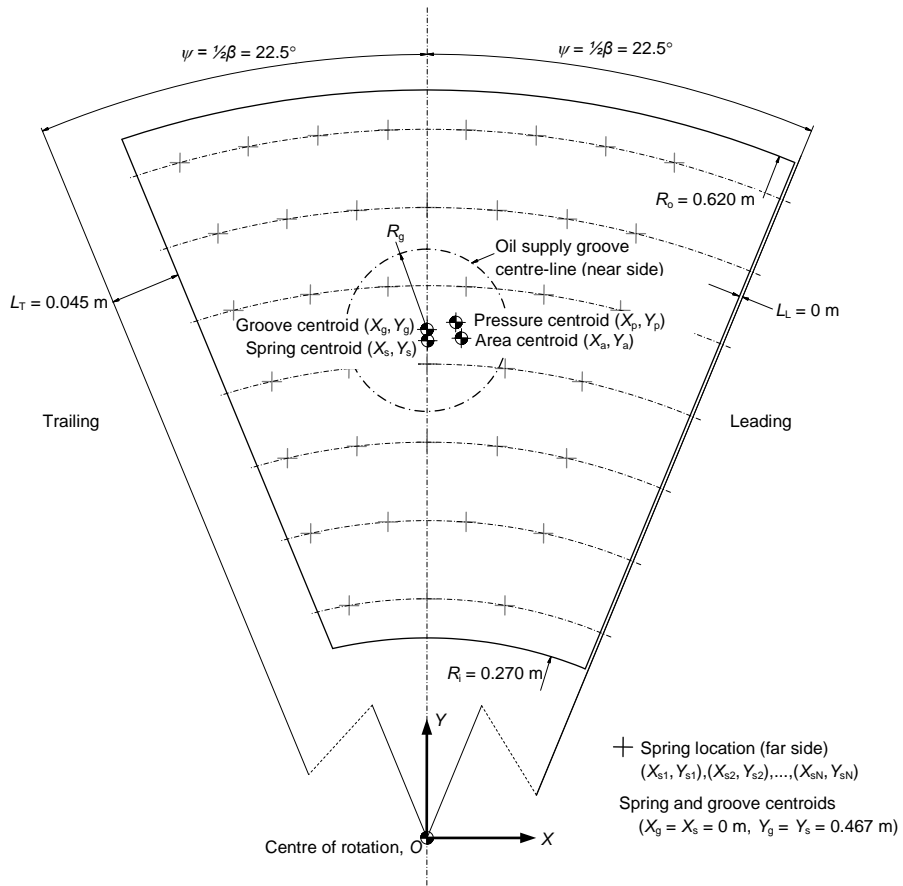


Fig. 2. Plan view of the truncated sector pad, showing nominal spring positions and groove location.

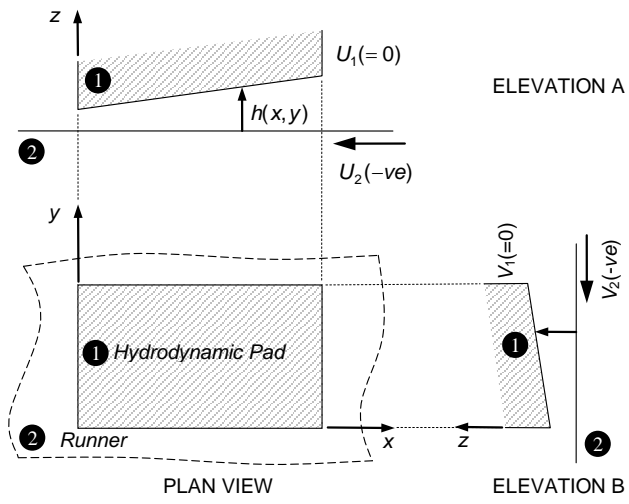


Fig. 3. Mathematical setup of bearing coordinate system.

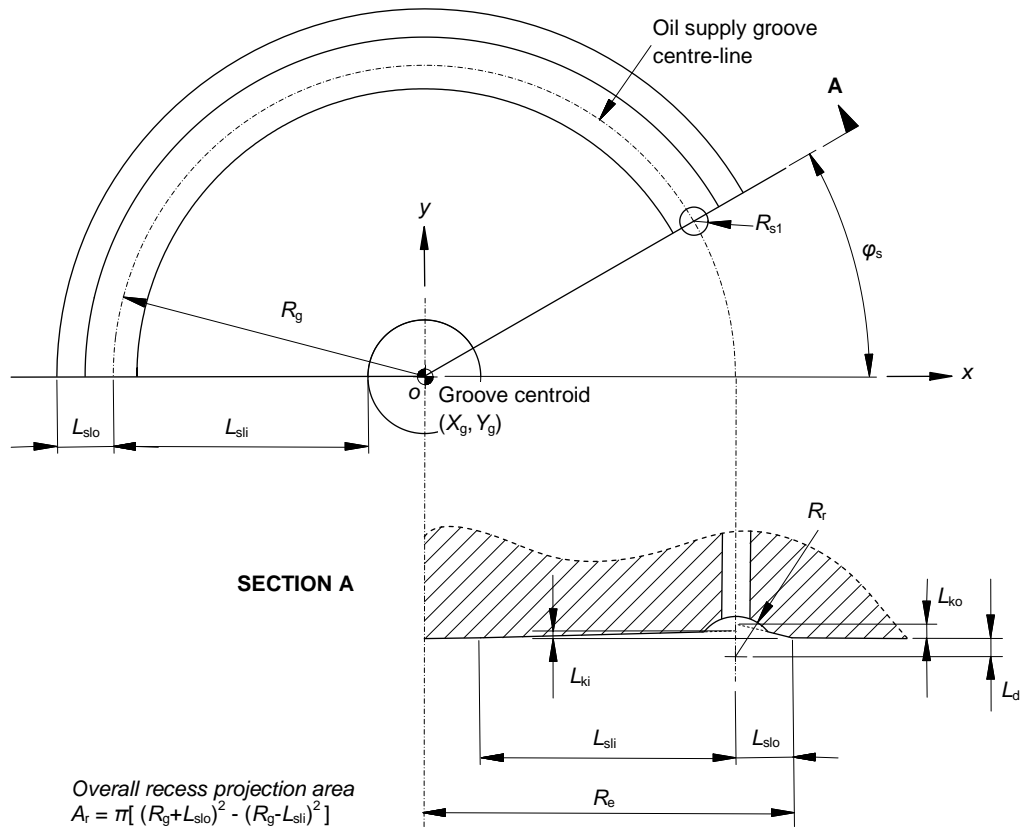
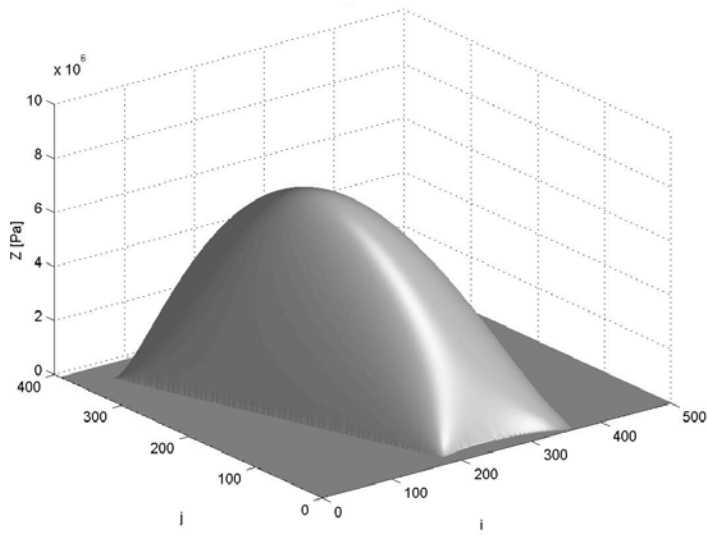
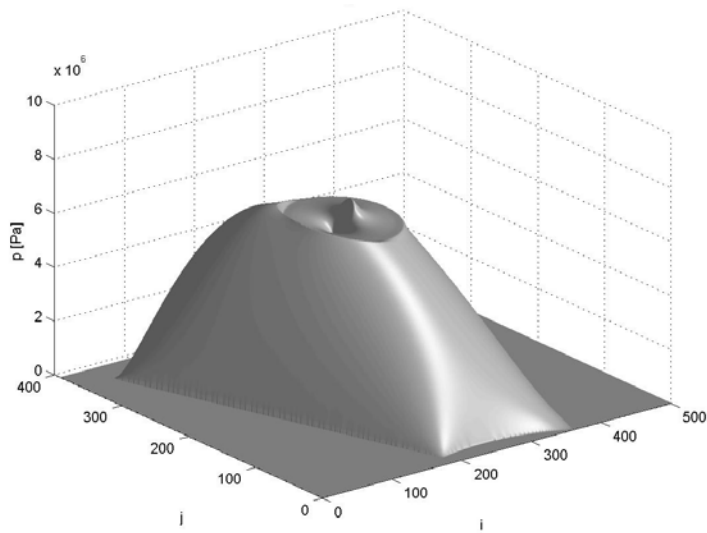


Fig. 4. Details of toroidal-segment oil supply groove with inner and outer tapered relief.



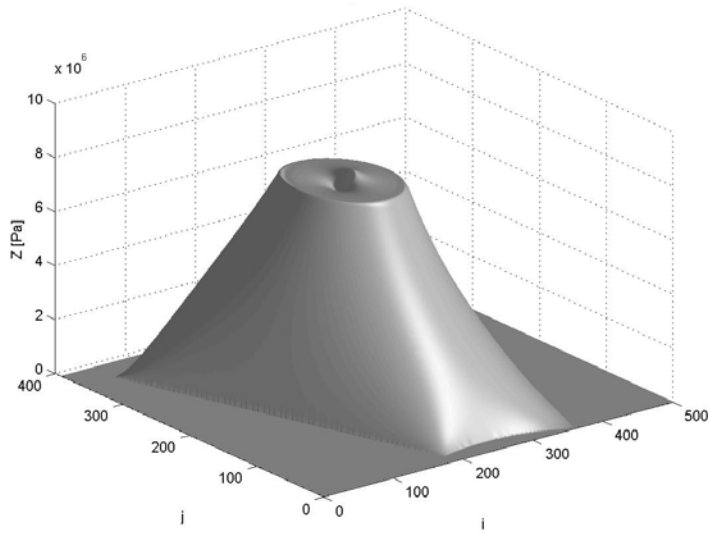
Pad load [kN]	340
Speed [rpm]	200
Oil temp [°C] (Viscosity [Pa·s])	50 (0.04)
h_{nom} (h_{min}) [μm]	59 (43)
K_{α}	0.65
$\Delta\theta$ [°K]	32
Π_p [kW]	6.8

Fig. 5(a) Rigid isoviscous pressure distributions for: (a) plane pad; (b) pad with type B recess; (c) pad with type B recess plus hydrostatic supply.



Pad load [kN]	340
Speed [rpm]	200
Oil temp [°C] (Viscosity [Pa·s])	50 (0.04)
h_{nom} (h_{min}) [μm]	62 (43)
K_{α}	0.73
$\Delta\theta$ [°K]	28
Π_p [kW]	6.1

Fig. 5(b) Rigid isoviscous pressure distributions for: (a) plane pad; (b) pad with type B recess; (c) pad with type B recess plus hydrostatic supply.



* Convective heat removal by hydrostatic oil supply not considered.

Pad load [kN]	340
Speed [rpm]	200
Pump pressure [MPa]	12.6
Oil flow [L/s]	4.2
Oil temp [°C] (Viscosity [Pa·s])	50 (0.04)
h_{nom} (h_{min}) [μm]	99 (64)
$\Delta\theta$ [°K]	13*
K_α	0.78
Π_p [kW]	3.4

Fig. 5(c) Rigid isoviscous pressure distributions for: (a) plane pad; (b) pad with type B recess; (c) pad with type B recess plus hydrostatic supply.

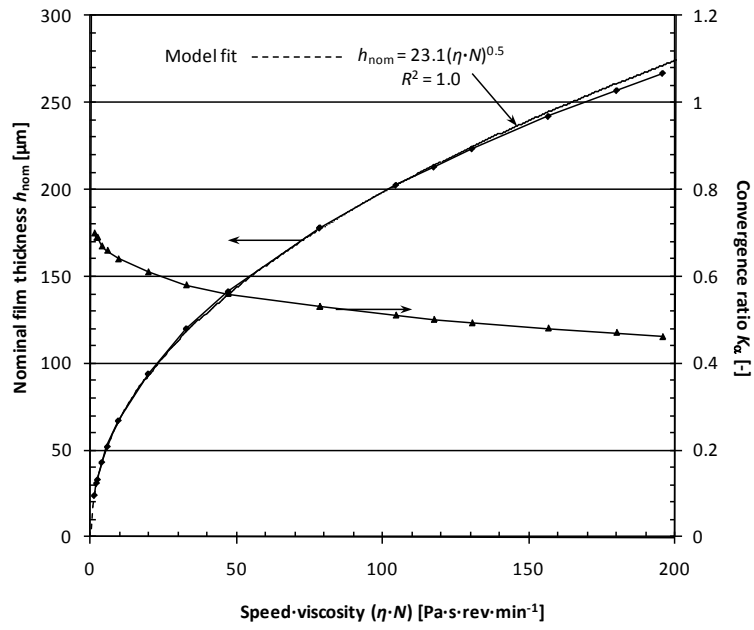


Fig. 6. Nominal film thickness and convergence for the plane (un-recessed) pad as a baseline for comparison with recessed pads.

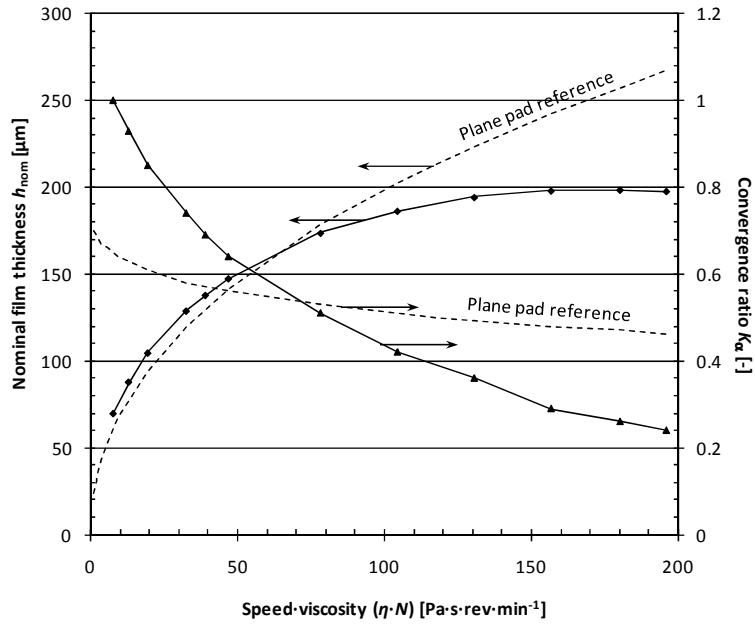


Fig. 7(a) Nominal film thickness and convergence performance of recessed pads relative to a plane pad:
 (a) recess type A; (b) recess type B; (c) recess type C.

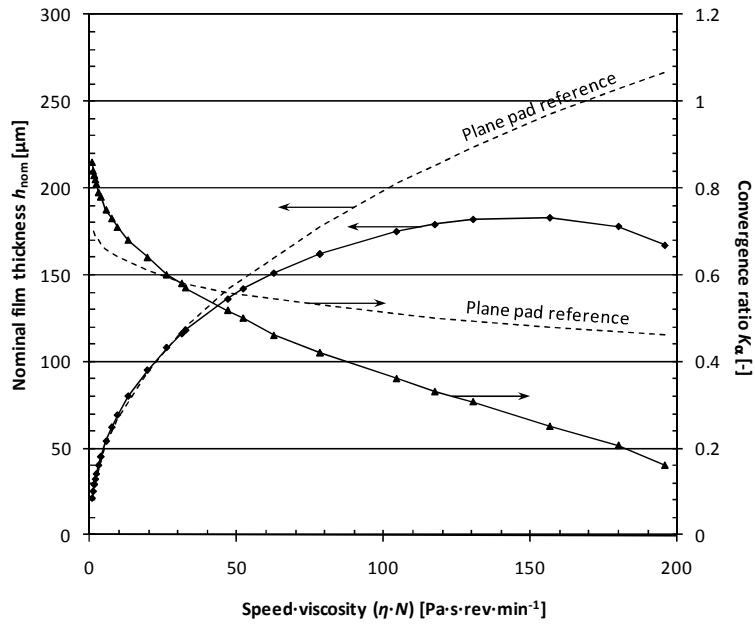


Fig. 7(b) Nominal film thickness and convergence performance of recessed pads relative to a plane pad: (a) recess type A; (b) recess type B; (c) recess type C.

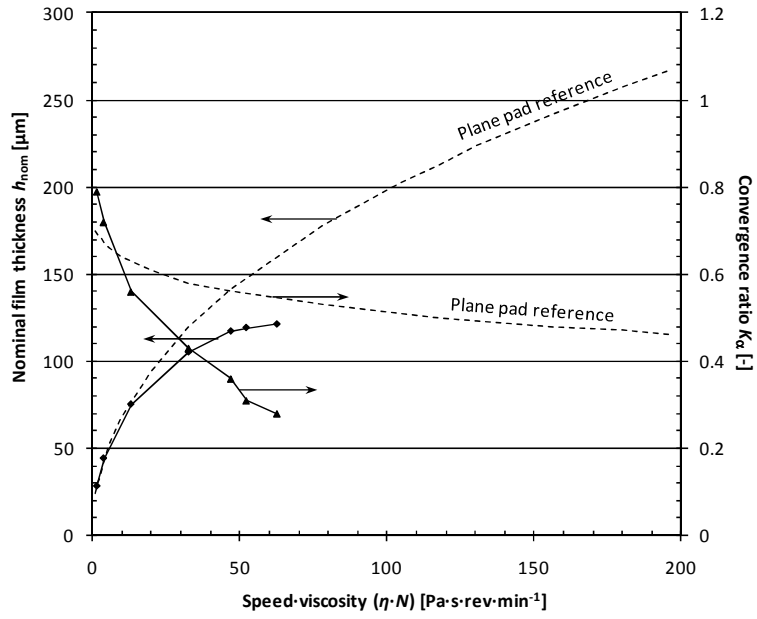


Fig. 7(c) Nominal film thickness and convergence performance of recessed pads relative to a plane pad: (a) recess type A; (b) recess type B; (c) recess type C.

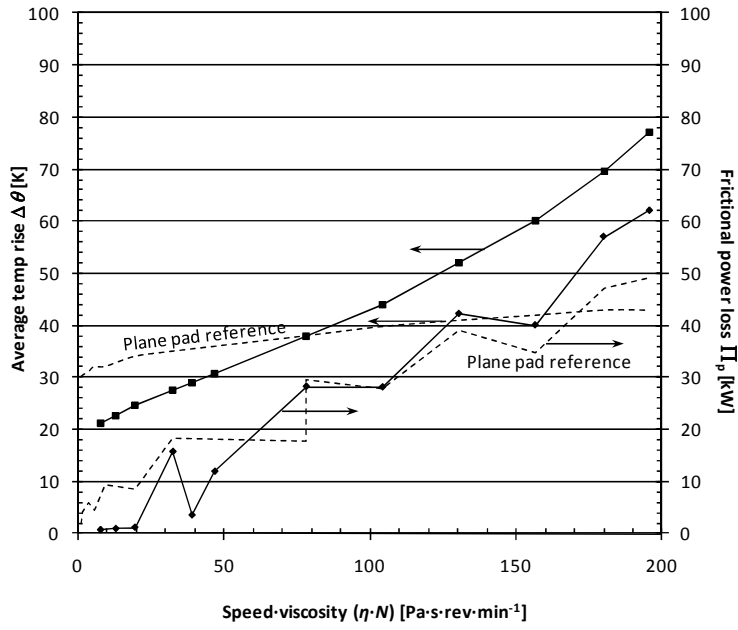


Fig. 8(a) Average oil film temperature rise and frictional power loss of recessed pads relative to plane pad: (a) recess type A; (b) recess type B; (c) recess type C.

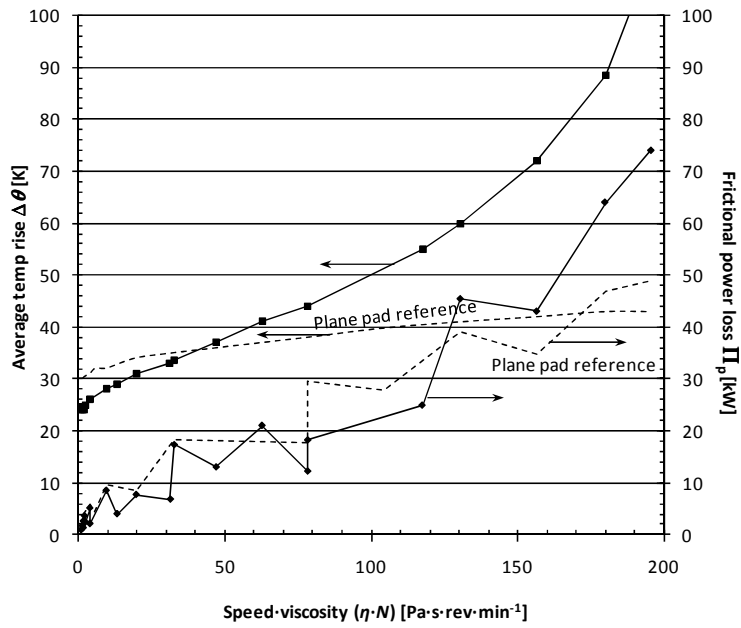


Fig. 8(b) Average oil film temperature rise and frictional power loss of recessed pads relative to plane pad: (a) recess type A; (b) recess type B; (c) recess type C.

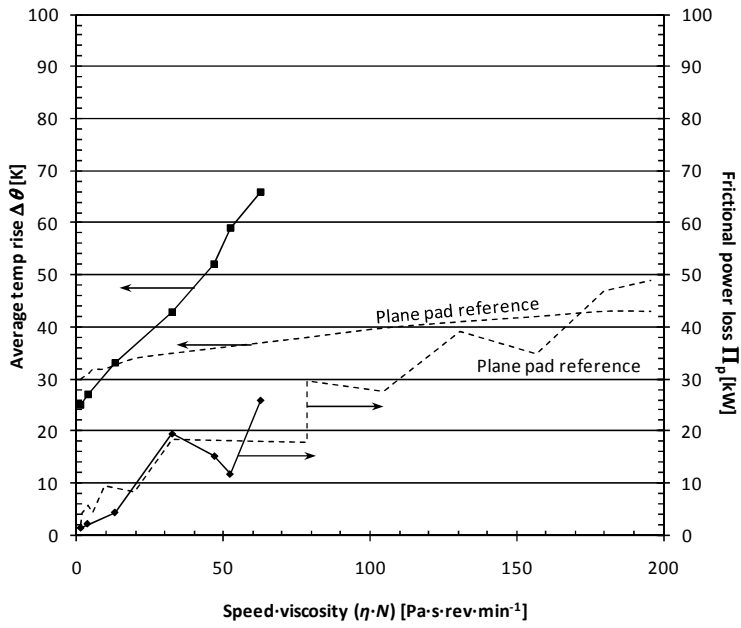


Fig. 8(c) Average oil film temperature rise and frictional power loss of recessed pads relative to plane pad: (a) recess type A; (b) recess type B; (c) recess type C.

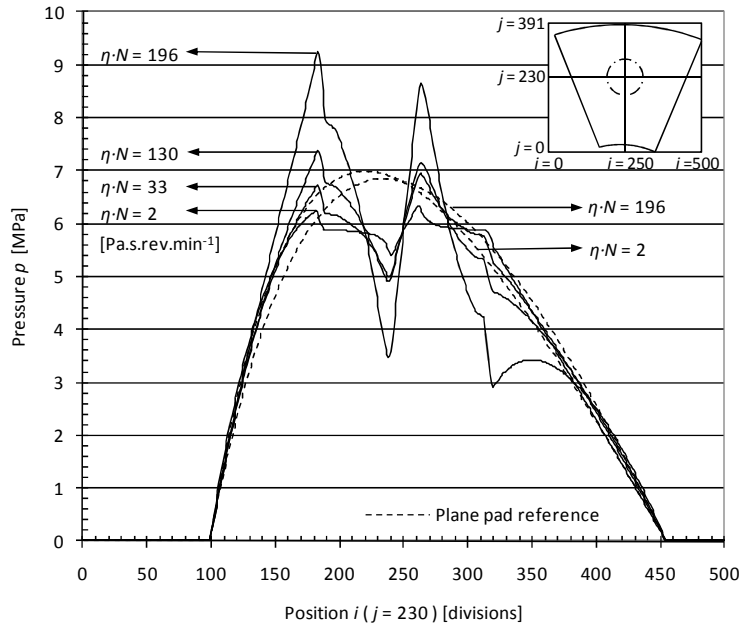
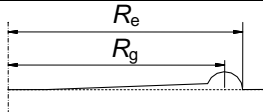

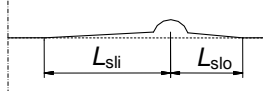


Fig. 9. The variation of pressure profile across the pad (recess type C) in the x -direction (trailing edge on the left) under hydrodynamic condition showing the effect of increasing speed or dynamic viscosity under isoviscous conditions.

Type		R_g	L_{slo}	L_{sli}	L_{ko}	L_{ki}
A		60	0	50	0	0.6
B		55	10	45	0.2	0.5
C		45	20	35	0.4	0.4

Common dimensions: $L_d = 7.6$ mm; $R_r = 9.1$ mm; $R_{s1} = 2.5$ mm; $\varphi_s = 30^\circ$; $R_e = 65$ mm; $A_r = 13,000$ mm².

Table 1. Geometry specification of the three recess types (A, B and C) tested. Refer to Fig. 4 for symbol definitions.

Temperature (°C)	Viscosity (cS)	Viscosity (Pa·s)
0	900	0.783
5	600	0.522
12	360	0.313
25	150	0.130
50	43	0.037
75	17	0.015
100	9	0.008

Table 2. Viscosity extrapolation of oil as per ASTM D341.